

ADVANCED ENERGY MATERIALS

Supporting Information

for *Adv. Energy Mater.*, DOI: 10.1002/aenm.202101636

Reimagining the e_g^1 Electronic State in Oxygen Evolution
Catalysis: Oxidation-State-Modulated Superlattices as a
New Type of Heterostructure for Maximizing Catalysis

*Ran Ding, Parisa Yasini, Haowei Peng, John P. Perdew,
Eric Borguet,* and Michael J. Zdilla**

Supporting Information

Reimagining the eg^1 electronic state in oxygen evolution catalysis: Oxidation-state-modulated superlattices as a new type of heterostructure for maximizing catalysis.

*Ran Ding, Parisa Yasini, Haowei Peng, John P. Perdew, Eric Borguet, * Michael J. Zdilla.**

R. Ding, P. Dr. Parisa Yasini, Prof. J. P. Perdew, Prof. E. Borguet, Prof. M. J. Zdilla, Prof. C. Department of Chemistry, Temple University, Philadelphia, PA 19112, USA.

E-mail: eborguet@temple.edu, mzdilla@temple.edu

Dr. H. Peng, Prof. J. P. Perdew, Department of Physics, Temple University, Philadelphia, PA 19112, USA.

Dr. H. Peng, Bluebell, PA 19422

Contents:

1. Assembly and characterization of few-layer catalysts.	3
2. TEM	5
3. Average Oxidation State from ICP-OES back titration.	6
4. XPS.....	7
5. Tafel Plots and Electrochemical Tables	7
6. STM/STS Additional Data	13

1. Assembly and characterization of few-layer catalysts.

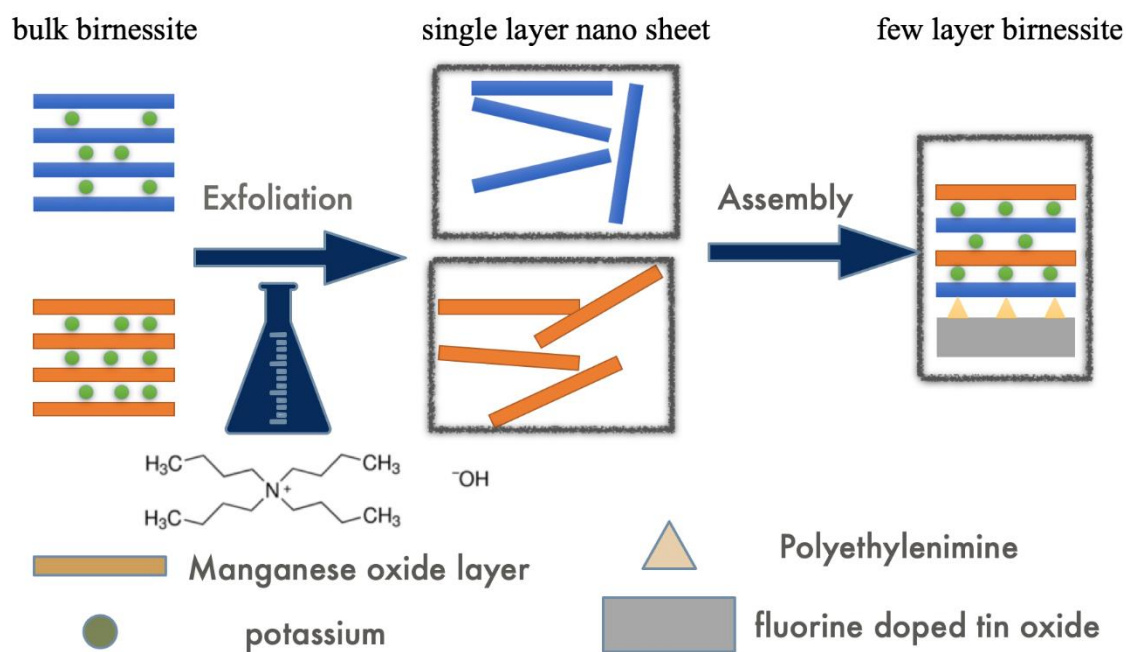


Fig. S1. Cartoon illustration of the exfoliation and reassembly process for controlled stacking of birnessite layers.

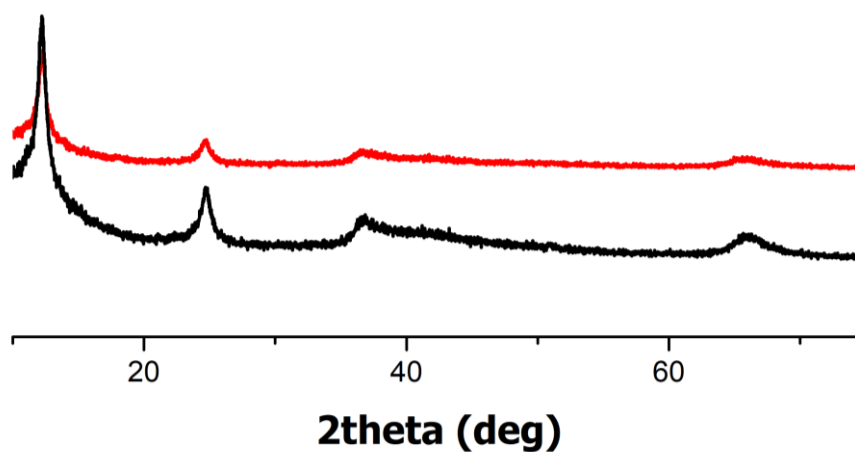


Fig. S2. PXRD pattern of pristine birnessite (black) and reduced birnessite (red) using Cu $K\alpha$ radiation.

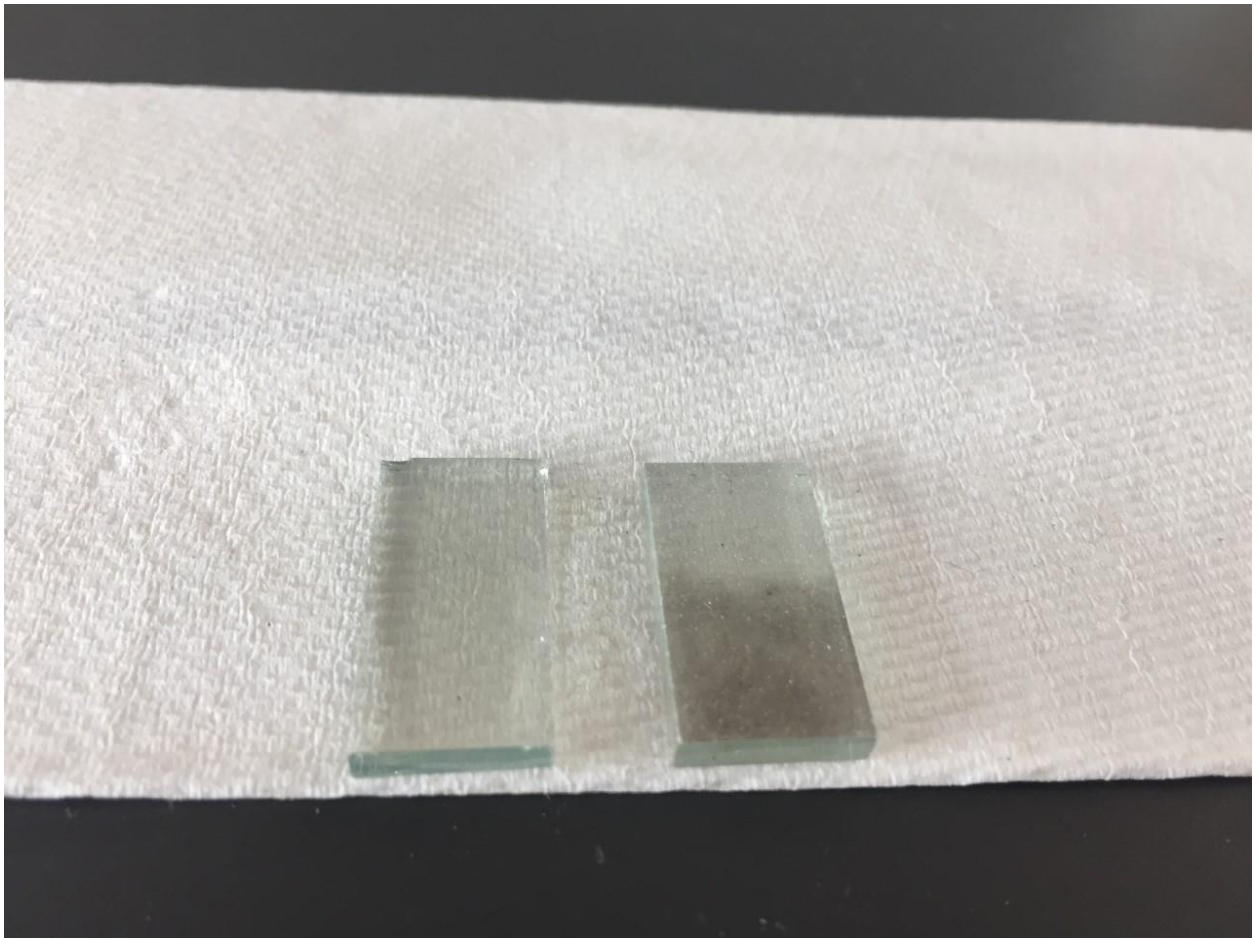


Fig. S3. Pictures of FTO before (left) and after (right) coated with few-layers of birnessite.

2. TEM

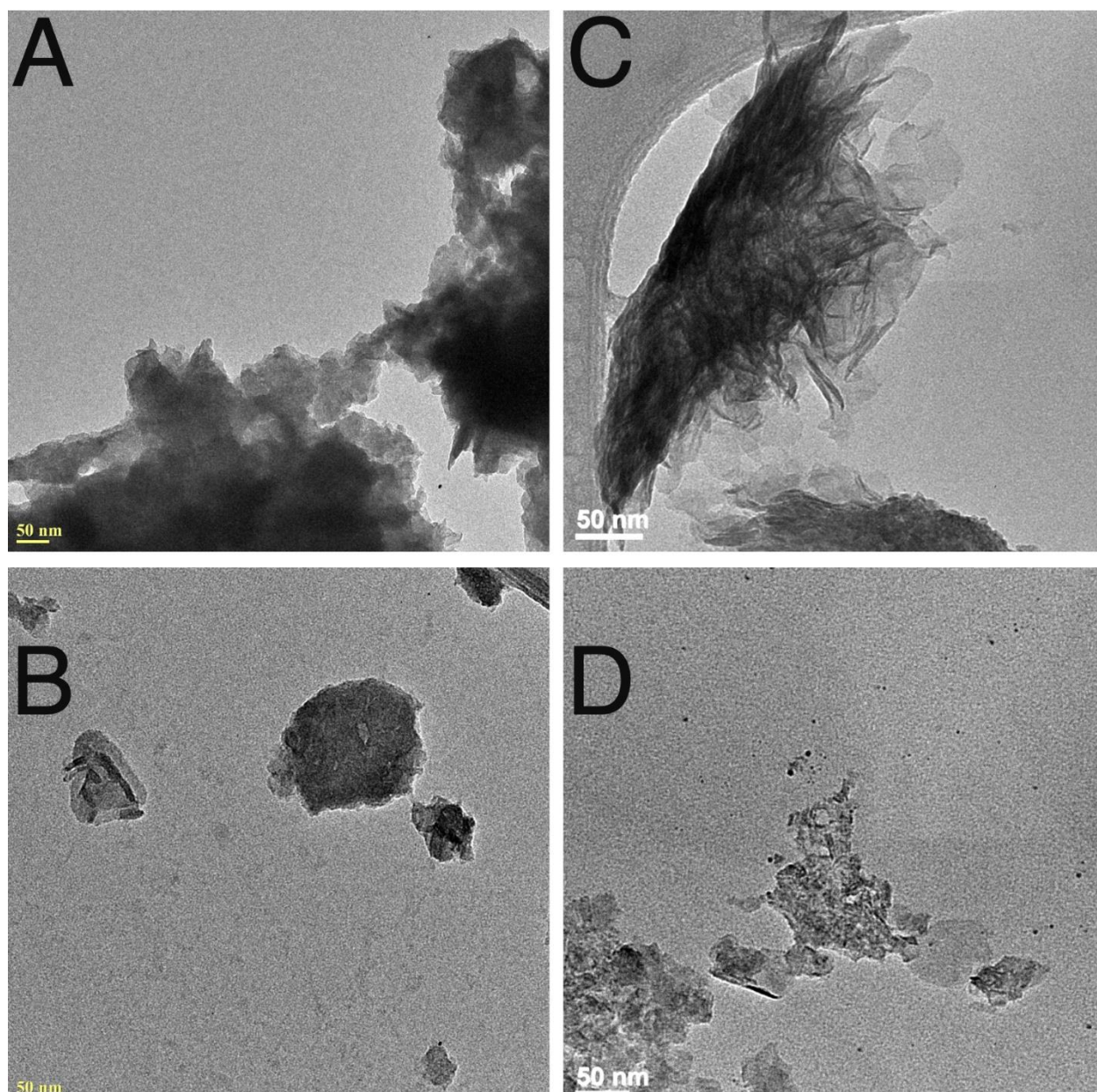


Fig. S4. TEM images of (A) pristine birnessite before exfoliation, (B) reduced birnessite before exfoliation, (C) NS of pristine birnessite after exfoliation, (D) NS of reduced birnessite after exfoliation.

3. Average Oxidation State from ICP-OES back titration.

Table S1. Manganese content for bulk birnessite sample determined by ICP-OES.

	Birnessite Digested (mg)	ICP Concentration (mg/L)	Mn Content (mg)	Mn Content (g Mn/ g birnessite)
Pristine birnessite	50.5	0.960	24.0	0.475
Reduced birnessite	50.0	0.916	22.9	0.458

Table S2. The AOS and stoichiometries of birnessite determined by ICP-OES and back titration.

	The amount of electrons (mmol) needed to reduce 1 g of birnessite to Mn(II)	AOS of Mn	Formula
Pristine birnessite	15.98	3.85	$K_{0.15}MnO_2$
Reduced birnessite	14.18	3.70	$K_{0.30}MnO_2$

4. XPS

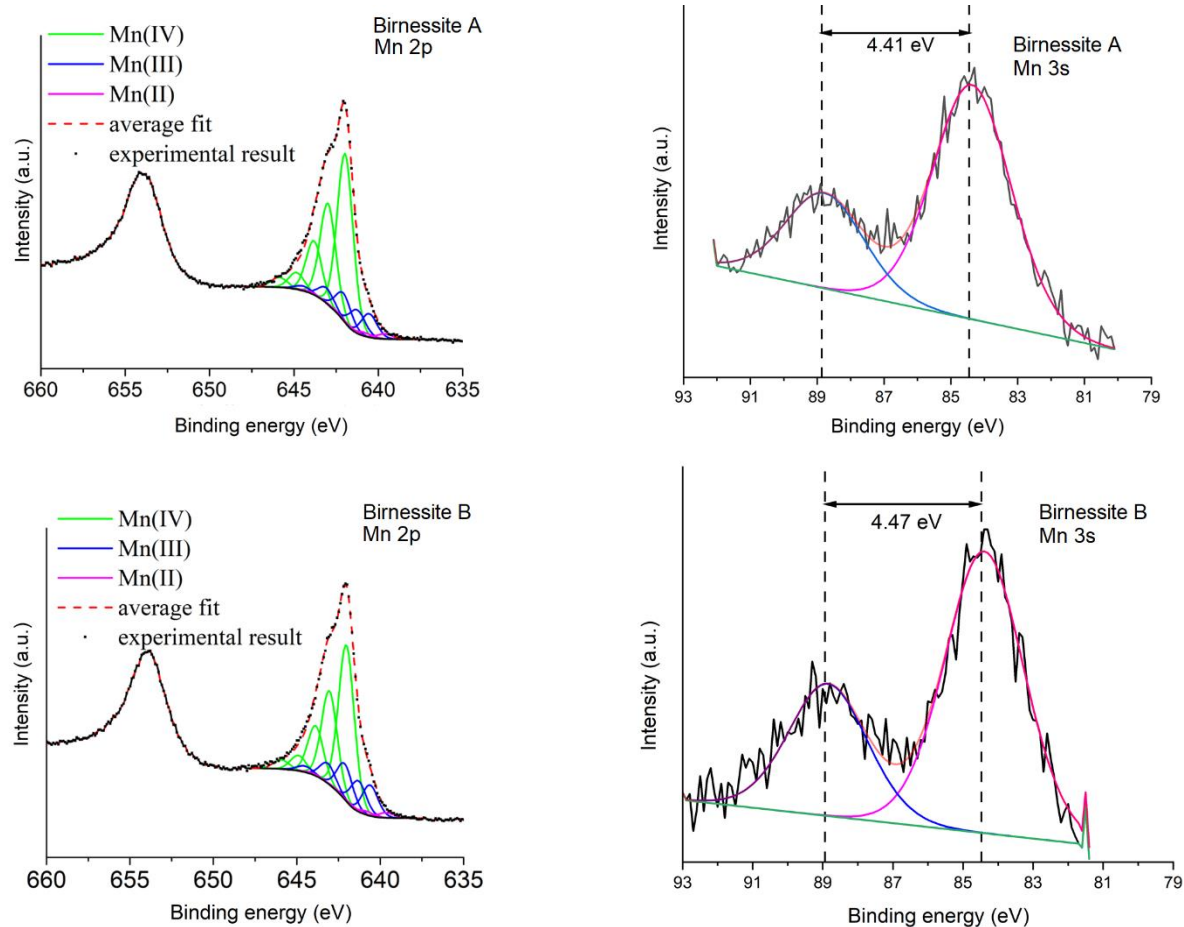


Figure S5. X-ray photoelectron spectra of the 2p electrons (left) and 3s electrons (right) of the manganese region of sample FAAAAAA (top) and FBBBBBB (bottom). AOS is examined by fitting of the 2p region. For FAAAAAA, AOS = 3.85 (top), and for FBBBBBB, AOS = 3.70 (bottom). The larger 3s splitting in Birnessite B is consistent with lower average oxidation state due to the increase in exchange energy and electron-electron repulsion in d^4 Mn^{III} in comparison to d^3 Mn^{IV} . “F” Designates the FTO electrode substrate. “A” and “B” represents monolayer of manganese oxide with different oxidation states. Spectra are fit^[43] to variable Mn(II)/(III)/(IV) signals to estimate relative content (see SI for values).

Table S3. XPS data for birnessite samples.

	AOS	Mn(IV) (%)	Mn(III) (%)	Mn(II) (%)
Pristine birnessite	3.77	79.38	18.62	2.00
Reduced birnessite	3.67	70.25	26.73	3.02

5. Tafel Plots and Electrochemical Tables

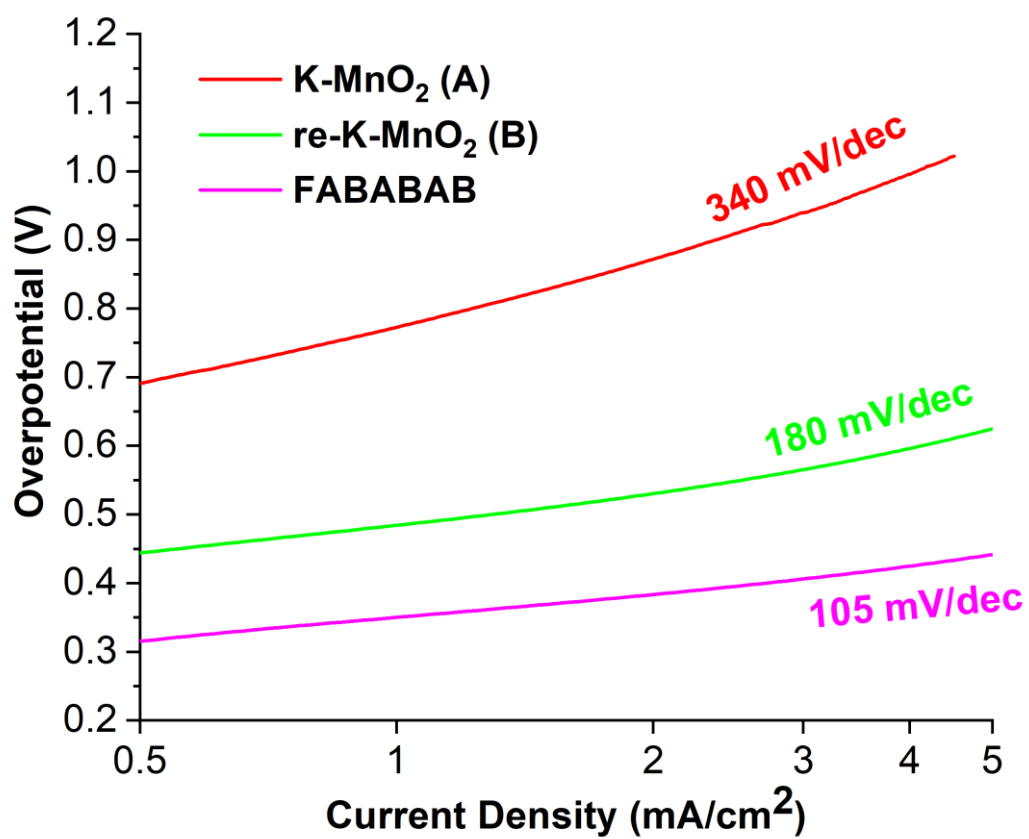


Fig. S6. Tafel slopes derived from the LSV curves in fig. 5 correspondingly.

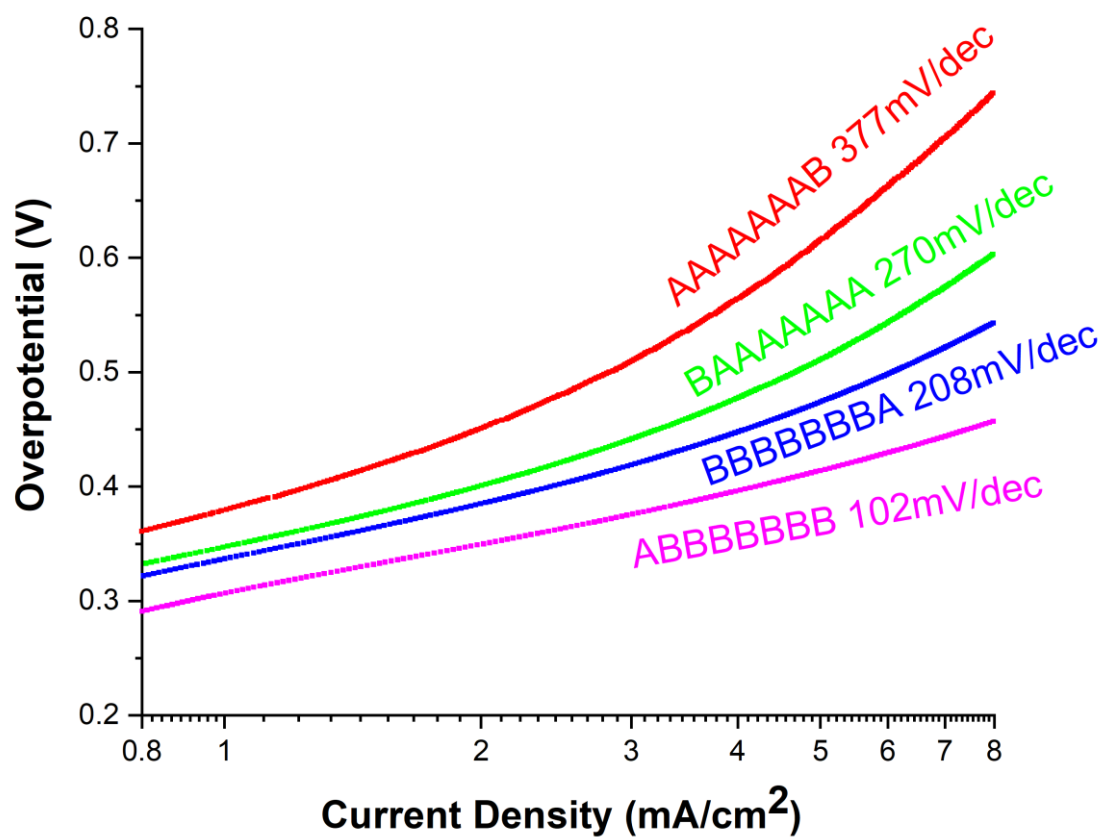


Fig. S7. Tafel slopes derived from the LSV curves in fig. 6A correspondingly.

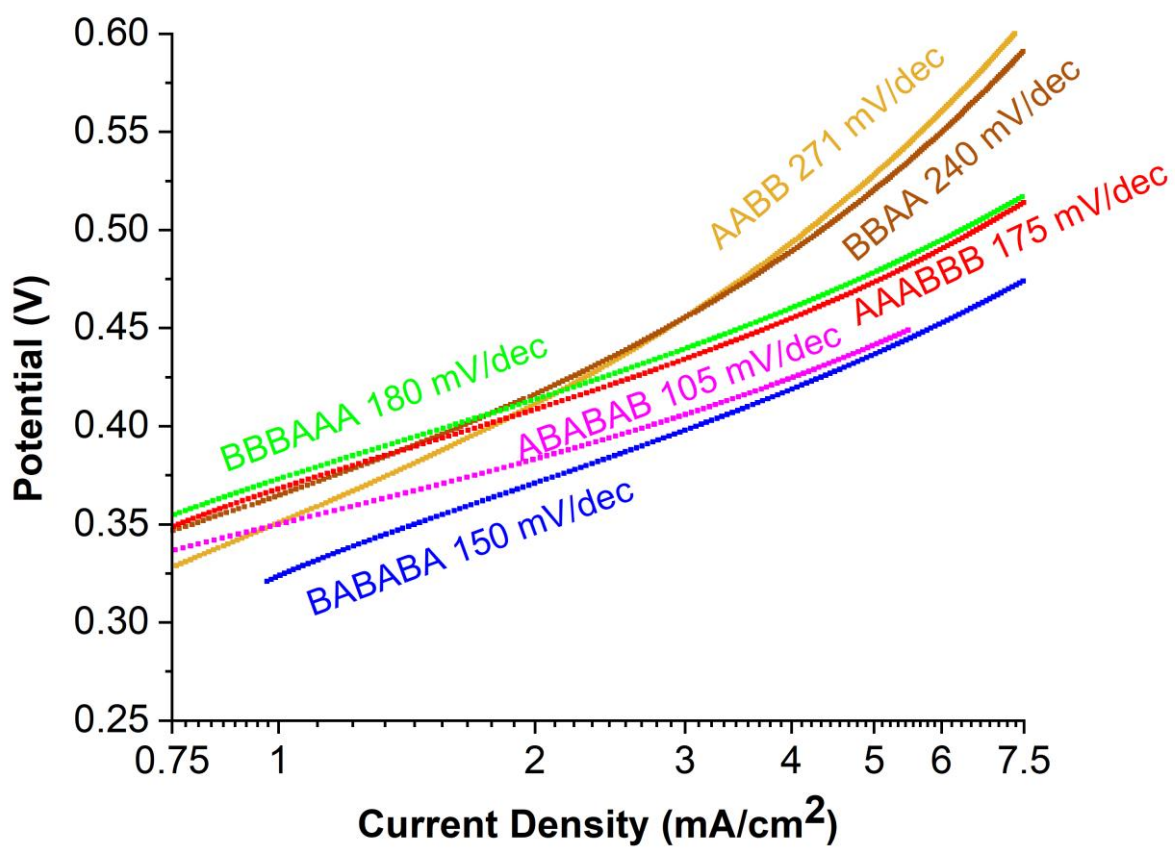


Fig. S8. Tafel slopes derived from the LSV curves in fig. 6B correspondingly.

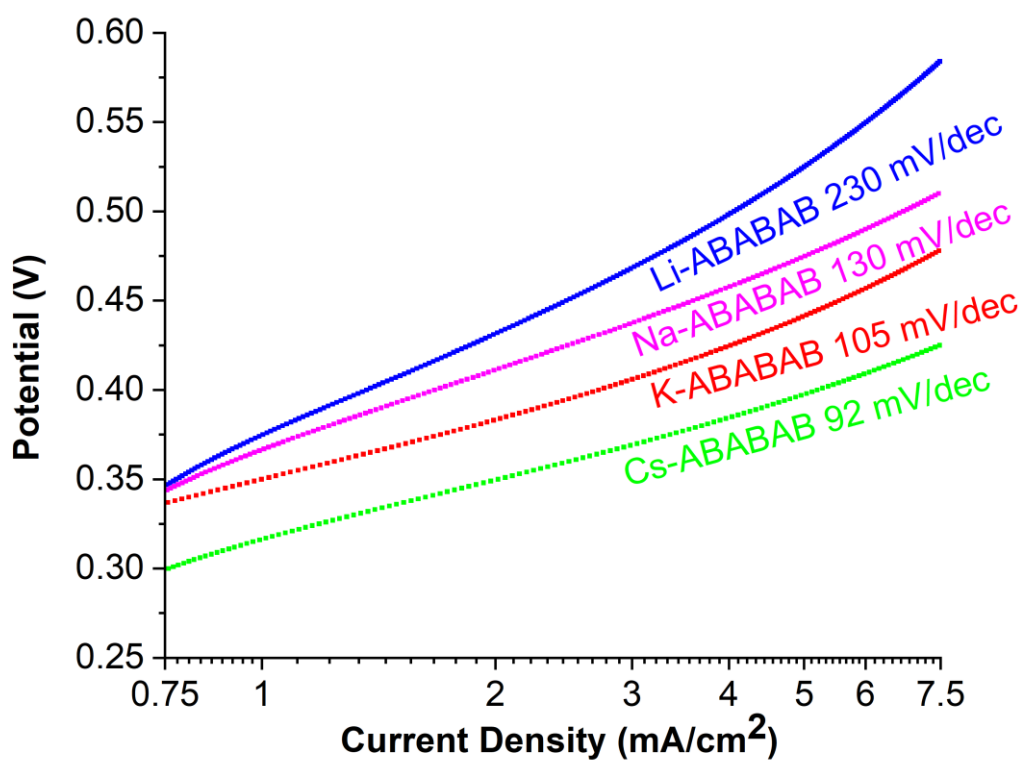


Fig. S9. Tafel slopes derived from the LSV curves in fig. 7 correspondingly.

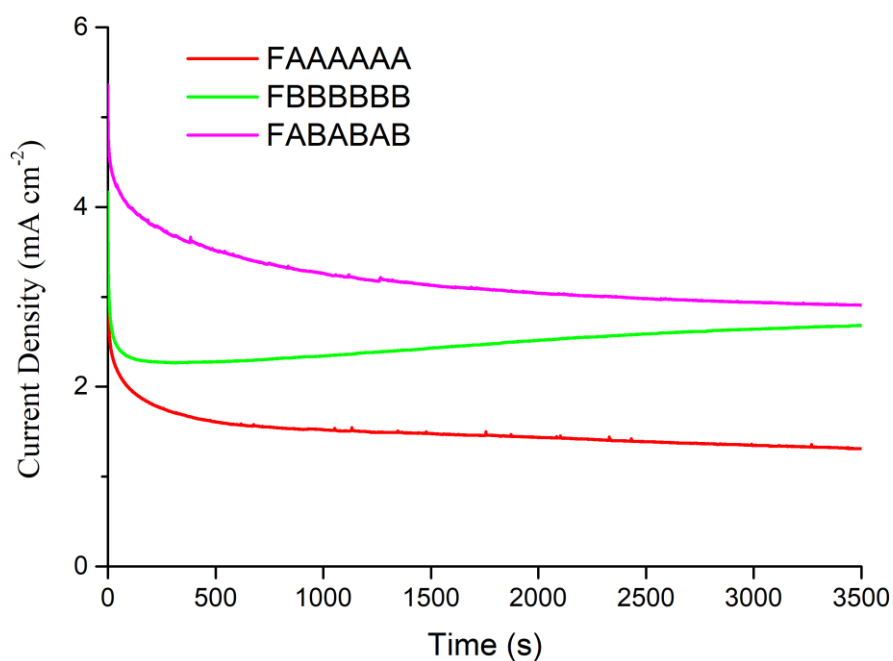


Figure S10. Chronoamperometry of the oxygen evolution reaction with FAAAAAA at a potential of 2.0 V versus RHE (red); FB BBBB at a potential of 1.85 V versus RHE (green); FABABAB at a potential of 1.7 V versus RHE (black).

Table S4. Summary of few-layer birnessite catalysts by electrochemistry.

Sample	Overpotential (mV)	Tafel Slope (mV/dec)
FAAAAAA	>1000	340
FBBBBBB	750	180
FABABAB	510	105
FBABABA	505	150
FAAABBB	550	175
FBBBAAA	550	180
FAABB	670	271
FBBA	650	240
FABBBBBBB	480	102
FBBBBBBBA	580	208
FAAAAAAAB	810	377
FBAAAAAAA	650	270
FABABAB with intercalated Li ⁺	640	230
FABABAB with intercalated Na ⁺	545	130
FABABAB with intercalated Cs ⁺	450	92

6. STM/STS Additional Data

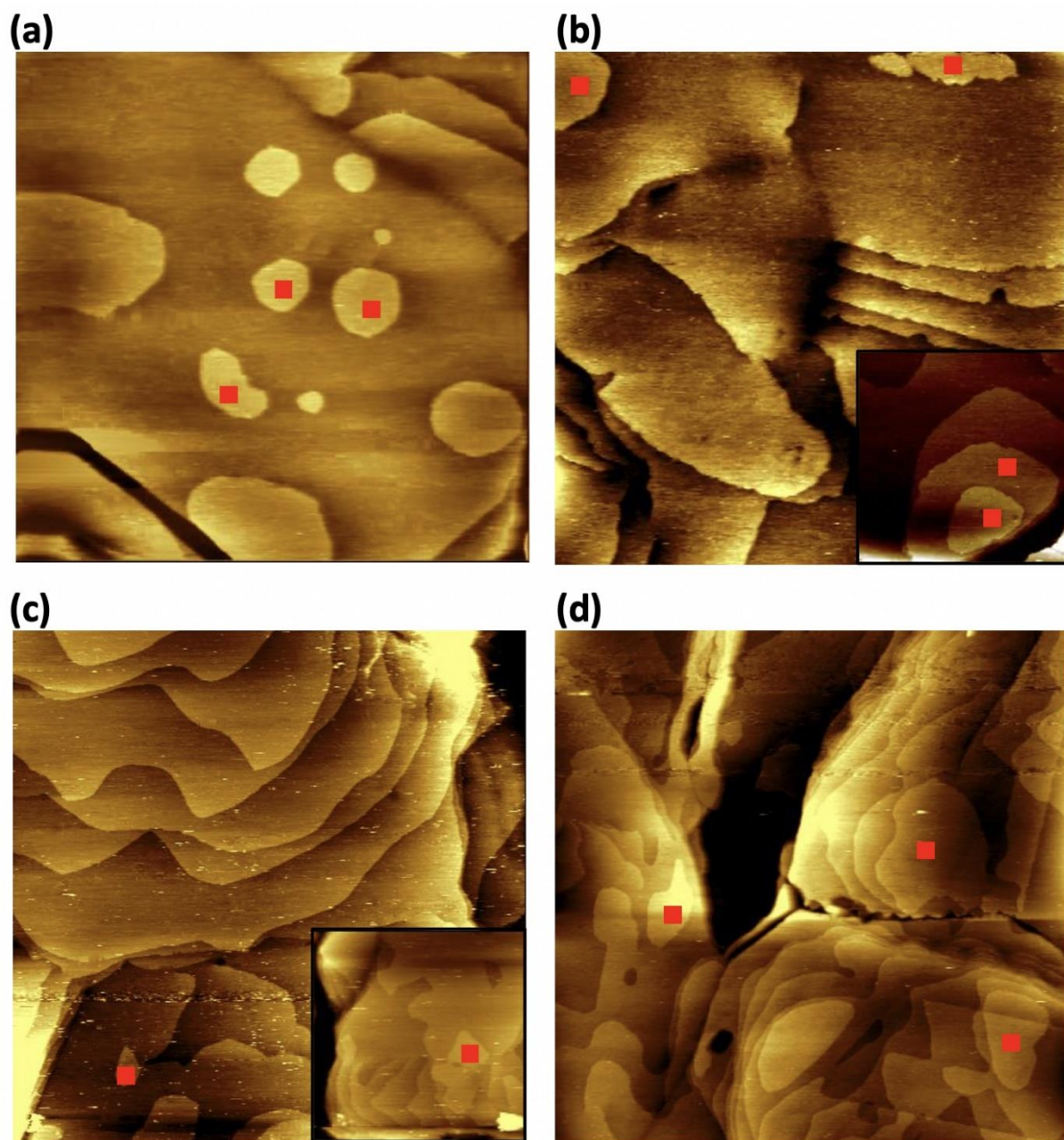


Figure S11: STM images of two-layer birnessite samples GAA, GBB, GAB and GBA. (a) GAA, $350 \times 350 \text{ nm}^2$, (b) GBB, $500 \times 500 \text{ nm}^2$, inset: another location: $300 \times 300 \text{ nm}^2$ (c) GAB, $1000 \times 1000 \text{ nm}^2$, inset: another location: $500 \times 500 \text{ nm}^2$ (d) GBA, $900 \times 900 \text{ nm}^2$. All the STM images were recorded in ambient temperature and pressure, $I_t=0.1 \text{ nA}$, $V_{\text{bias}}=0.3 \text{ V}$. Locations of the tip for STS measurements indicated with red rectangles.

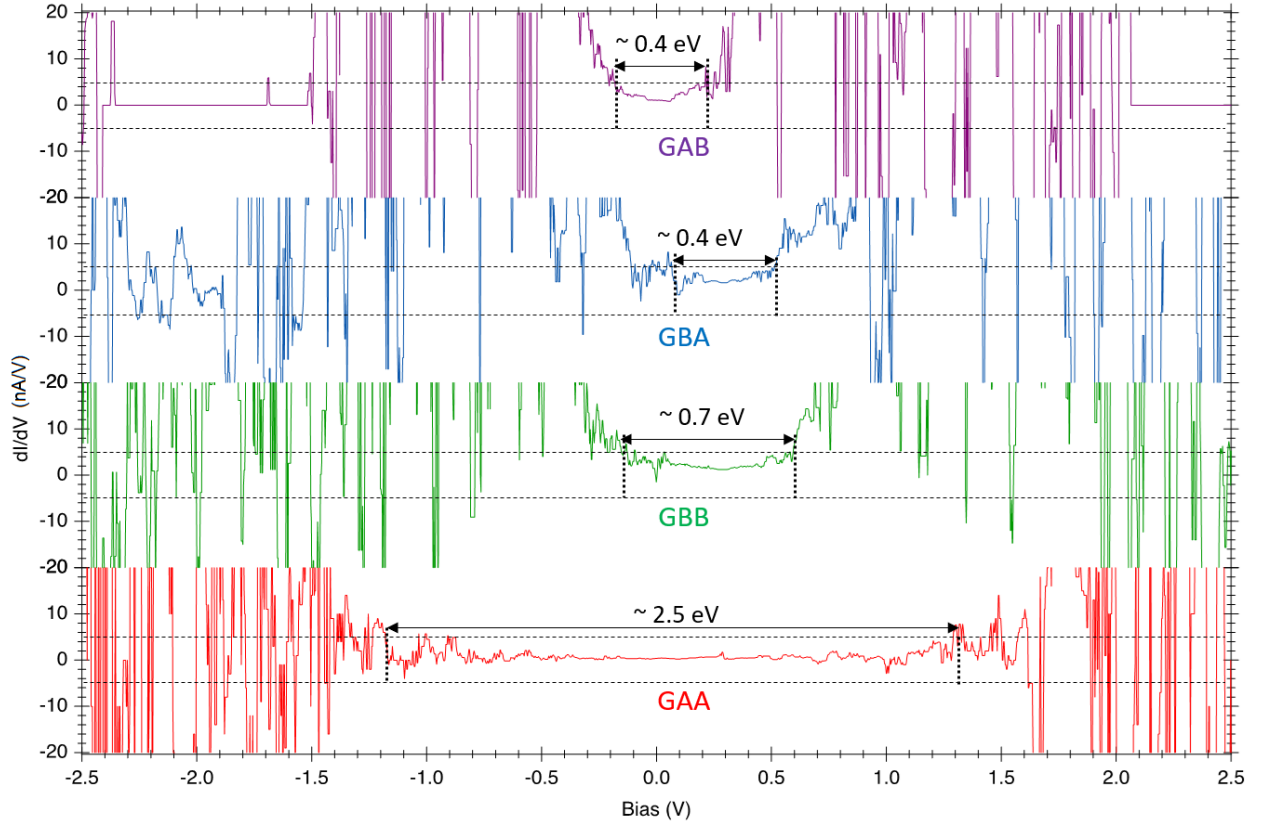


Figure S12. Bandgap estimation from plot of dI/dV of experimental STS (Fig. 8, top). Bandgap threshold current set at ± 5 nA.

Fitting of STS

The GAA STS spectrum was fitted to the equation:

$$f(x) = Y_0 + A_1 e^{-\frac{x-x_0}{\tau_1}} + A_2 e^{-\frac{x-x_0}{\tau_2}} + (Y_1 + A_3 e^{Bx}) \quad (1)$$

The GBB, GAB, and GBA spectra were fit to the equation:

$$f(x) = Y_0 + \left\{ \frac{M_0}{1 + e^{\frac{(h_0-x)}{R_0}}} \right\} + Y_1 \quad (2)$$

The experimentally determined parameters are given in Tables S5 and S6.

Table S5

	Parameters								
AA	Y_0	A_1	τ_1	A_2	τ_2	Y_1	A_3	B	x_0
	-0.06	-31.01	0.44	0.05	18.10	-0.13	0.05	2.31	-2.55

Table S6

	Parameters							
	Y_0	M_0	h_0	R_0	Y_1	M_1	h_1	R_1
BB	0.35	-55.00	1.16	-0.16	-4.64	59.34	-0.77	0.17
AB	-1.81	-50.34	0.65	-0.07	-47.10	100.16	-0.84	0.15
BA-Sonication	0.34	-85.36	1.56	-0.26	2.86	81.83	-0.75	0.18
BA-TBAOH	0.41	-63.02	1.33	-0.25	8.56	54.10	-1.10	0.21